

A Novel Method for Thermoelectric Generator Based on Neural Network

Mohammad Sarairoh^{1,*}, A. M. Maqableh², Manar Jaradat³ and Omar A. Saraereh⁴

¹Mechanical Engineering Department, Faculty of Engineering, Mutah University, Karak, 61710, Jordan

²Electromechanical Engineering Department, Luminus Technical University College, Amman, 11118, Jordan

³Department of Computer Engineering, Faculty of Engineering, The Hashemite University, Zarqa, 13133, Jordan

⁴Department of Electrical Engineering, Faculty of Engineering, The Hashemite University, Zarqa, 13133, Jordan

*Corresponding Author: Mohammad Sarairoh. Email: maqsarairoh@mutah.edu.jo

Received: 15 March 2022; Accepted: 14 April 2022

Abstract: The growing need for renewable energy and zero carbon dioxide emissions has fueled the development of thermoelectric generators with improved power generating capability. Along with the endeavor to develop thermoelectric materials with greater figures of merit, the geometrical and structural optimization of thermoelectric generators is equally critical for maximum power output and efficiency. Green energy strategies that are constantly updated are a viable option for addressing the global energy issue while also protecting the environment. There have been significant focuses on the development of thermoelectric modules for a range of solar, automotive, military, and aerospace applications in recent years due to various advantages including as low vibration, great reliability and durability, and the absence of moving components. In order to enhance the system performance of the thermoelectric generator, an artificial neural network (ANN) based algorithm is proposed. Furthermore, to achieve high efficiency and system stability, a buck converter is designed and deployed. Simulation and experimental findings demonstrate that the suggested method is viable and available, and that it is almost similar to the real value in the steady state with the least power losses, making it ideal for vehicle exhaust thermoelectric generator applications. Furthermore, the proposed hybrid algorithm has a high reference value for the development of a dependable and efficient car exhaust thermoelectric generating system.

Keywords: Thermoelectric system; thermodynamics; electromechanics; rotational factors; neural networks

1 Introduction

The engine is the core component of traditional fuel vehicles and gasoline-electric hybrid electric vehicles, while only about 30% of the energy of the commonly used gasoline engine is used to drive the vehicle and to be used for on-board electrical appliances during the work process, and about 40% of the energy is in the form of waste heat. The exhaust gas is emitted, and the average temperature



This work is licensed under a Creative Commons Attribution 4.0 International License, which permits unrestricted use, distribution, and reproduction in any medium, provided the original work is properly cited.

of the exhaust pipe exceeds 250°C [1,2]. It is particularly important to improve the fuel efficiency of traditional fuel vehicles and hybrid electric vehicles and reduce harmful gas emissions. Therefore, the research on the vehicle exhaust thermoelectric power generation system is of great significance. It is to install a thermoelectric power generation module on the surface of the vehicle exhaust pipe to convert waste heat energy into electricity. The DC/DC converter stores the electrical energy in the battery [3]. At present, the research on on-board exhaust gas thermoelectric power generation mainly focuses on the modeling of thermoelectric modules [4], the design and improvement of the heat transfer performance of the thermal energy box [5,6], and the improvement of the topological connection of the thermoelectric modules [7].

The output power of the automotive exhaust thermoelectric generator (AETEG) is mainly affected by the engine operating conditions and external loads. When the engine is working at a stable speed, the power value of the thermoelectric generator increases with the voltage. The growth first increases and then decreases, so there is a maximum power point [8]. The research of maximum power tracking (MPPT) focuses on photovoltaic power generation systems, including disturbance-based self-optimization algorithms, intelligent processing methods and the combination of various methods [9]. Reference [10] proposed an improved variable-step conductance increment method, using the step-size adjustment coefficient $S = |dP/dV|/I$ to dynamically adjust the step-size change ΔU_{ref} , and at the same time to ensure the convergence of the algorithm, it is stipulated that $S < 1$, but the constant ΔU_{ref} cannot be changed once it is selected, and it is only suitable for specific external conditions. Reference [11] proposed a zero-average conductance incremental method, which ensures $dP_{PV}/dV_{PV} = 0$ in one switching cycle to reduce oscillation, but the selection of the boundary error e is a difficult problem, and if e is too large, the oscillation cannot be reduced. If e is too small, it is no different from the traditional conductance increment method. Reference [12] proposed a new BP neural network MPPT algorithm. The simulation results show that compared with the traditional conductance incremental method and disturbance observation method, the proposed algorithm has higher efficiency and smaller oscillation in steady state. But the number of required inputs (light intensity, temperature) is large. Reference [13] proposed a new direct adaptive neural network MPPT method. The online process is a learning algorithm based on the σ rule. Compared with the traditional interference observation method, its dynamic performance is greatly improved and the steady state fluctuation is greatly reduced. In addition, some scholars have designed a simple MPPT hardware circuit to reduce the loss of the converter and improve the output power of the system [14,15].

Literature [9–13] mainly studies the MPPT strategy of photovoltaic systems, but the power-voltage output characteristics of AETEG are quite different from those of photovoltaic cells (its temperature changes slowly). This paper proposes a novel approach method based on the above method. The enhanced conductance increment technique and the adaptive variable step size BP neural network approach are combined in the novel hybrid method. In the first stage, the improved conductance incremental method can quickly run at the reference point near the maximum power point. In the second stage, the MPPT controller of the BP neural network method with adaptive variable step size eliminates the vibration near the maximum power point in steady state. In order to be suitable for the AETEG system, an MPPT two-phase interleaved Buck converter with a series lag link is also designed. Both the Bode diagram and the root locus diagram show that the stable and dynamic performance of the MPPT controller with voltage closed loop is better than before. Simulation and experiments. The results demonstrate that the new hybrid method has fast tracking speed without additional circuitry and no additional power loss.

2 System Model

2.1 General Structure of AETEG's New Power Supply

The structure diagram of AETEG system is shown in Fig. 1, which includes a thermal energy box, two thermoelectric conversion modules and an independent refrigeration system. Among them, the high temperature side of the thermoelectric module (TEM) is in contact with the thermal energy tank, and the low temperature side is connected with the cooling water tank. The exhaust gas outlet of the engine is connected with the inlet of the thermal energy air box for heat transfer, the exhaust gas passes through the thermal energy air box, and the exhaust pipe is passed into the atmosphere. Meanwhile, the cooling system has a water tank, two valves and an air-cooled water pump. Due to the soft output characteristics of thermoelectric devices, as the output current increases, the output voltage drops sharply, which cannot match the power supply voltage level of the load. A DC/DC converter needs to be connected to 48 V. The battery supplies power to the electrical appliances in the car.

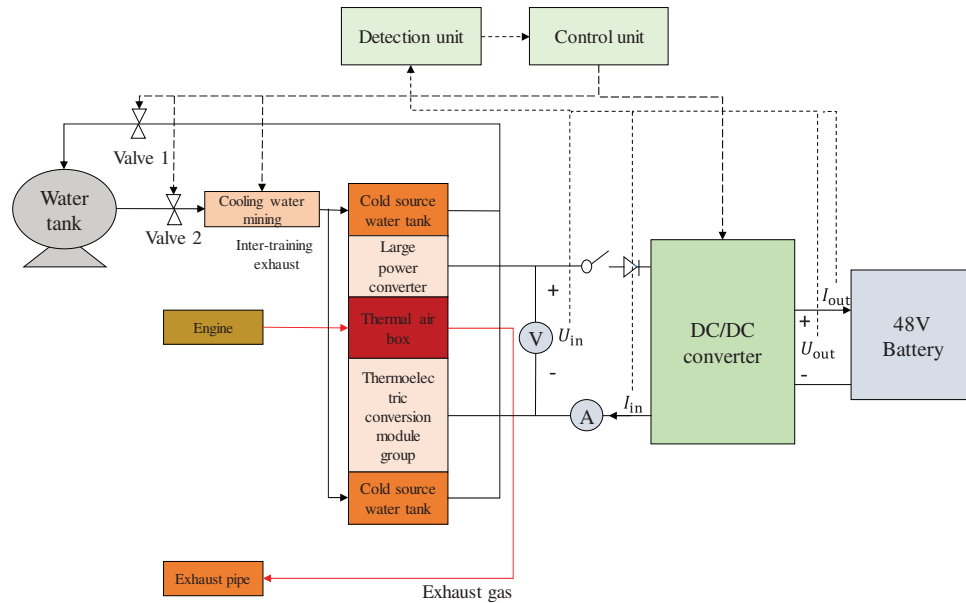


Figure 1: General structure of the new power supply in the proposed model

2.2 TEM Circuit Characteristics

Fig. 2 shows the circuit model of a single thermoelectric power generation device TEM, from which it can be obtained that the open circuit voltage and output power of the TEM are functions of the load and the temperature difference between the hot and cold ends [16], as shown below

$$U_{OC} = n\alpha_{PN}\Delta T = n\alpha_{PN}(T_H - T_L) \quad (1)$$

$$P_L = U_L I_L = \frac{n^2 \alpha_{PN}^2 (T_H - T_L)}{(R_{in} + R_L)} \times R_L \quad (2)$$

$$R_{in} = n\rho \left(\frac{l_N}{A_N} + l_p/A_p \right) \quad (3)$$

where α_{PN} is the Seebeck coefficient, which is related to the temperature gradient and installation pressure, ΔT is the temperature difference between the hot and cold ends of the TEM, and n is the number of thermocouples. In Eq. (3), ρ is the resistivity, l_N and l_P are the lengths of the N and P-type galvanic arms of the TEM, respectively, and A_N and A_P are the cross-sectional areas of the N and P-type galvanic arms, respectively. Usually, TEMs are connected in series to form a thermoelectric generator (assuming the number of TEMs is M), and the open-circuit voltage and internal resistance are respectively [17].

$$U_{\text{TEG}} = \sum_{i=1}^M U_{\text{OC}}(i) \quad (4)$$

$$R_{\text{TEG}} = \sum_{i=1}^M R_{\text{in}}(i) \quad (5)$$

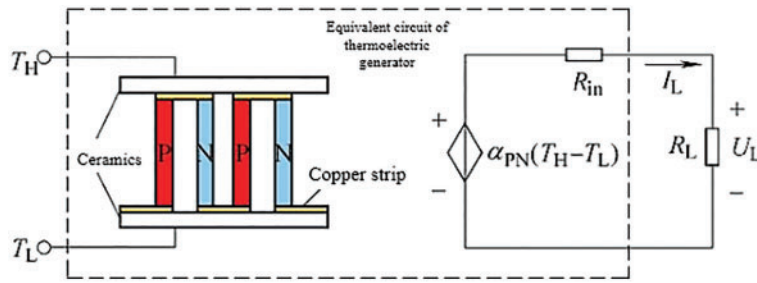


Figure 2: TEM equivalent circuit diagram

According to the power transfer theorem, when $R_L = R_{\text{TEG}}$, the load R_L obtains the maximum power, as shown in Eq. (6)

$$P_{\text{Lmax}} = \frac{U_{\text{TEG}}^2}{4R_{\text{TEG}}} \quad (6)$$

In the AETEG test bench, the I-U-P characteristic curve of the thermoelectric generator is shown in Fig. 3. When the temperature difference is stable, its output power-current curve has only one extreme point, that is, the maximum power point.

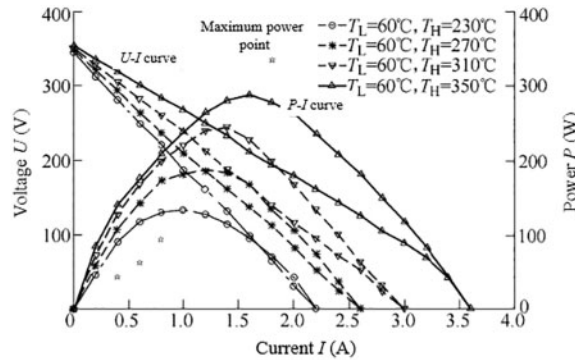


Figure 3: I-U-P characteristic curves of different heat source temperatures when the cold source temperature is 60°C

2.3 TEM Circuit Characteristics

Generally, the DC/DC converter supplies power to the battery with low voltage and high current. However, high current will cause a series of problems (high current stress, more conduction loss of the switch), and at the same time, the current ripple on the input and output sides will adversely affect the thermoelectric generator and battery. In order to reduce the current ripple on the input side, the inductor should work in the current continuous mode, but the inductor value will be very large, and its weight and volume will increase sharply, so a two-phase interleaved Buck converter is used [18–20]. Fig. 4 shows that a digitally controlled DC/DC converter is connected between AETEG and a 48 V LiFeO4 battery, and can implement the MPPT algorithm. The driving signals of the two switches Q1 and Q2 are shown in Fig. 5. They are generated by the PWM module in the DSP chip TMS320F28335, and the phase angle is staggered by 180° . The inductor currents I_{L1} and I_{L2} are half of the load current I_{out} , and the inductance values of L_1 and L_2 are becomes smaller, and the total current ripple is smaller than the single-phase ripple [18].

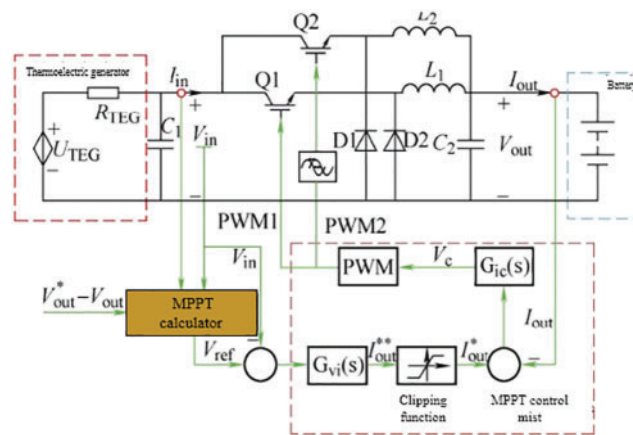


Figure 4: Staggered Buck topology and MPPT control structure

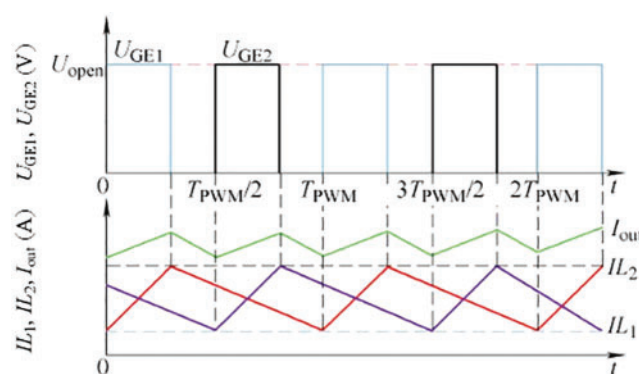


Figure 5: Circuit operating waveform in inductor current continuous mode

The DC/DC converter system is a nonlinear time-varying system, and the general linear theory cannot be directly applied. In order to carry out dynamic characteristic analysis and related design, the state space averaging method is used [19]. Ideally, two-phase interleaved Bucks can be regarded as the addition of two single-phase Bucks. According to the working process of the single Buck circuit, the state vector $\mathbf{x} = (U_{in} I_L U_o)$ is selected, which is the output voltage of the thermoelectric generator, the filter inductor current and the load side voltage. The input vector $\mathbf{u} = (I_{in})$ is the output current of the thermoelectric generator. The output vector $\mathbf{y} = (U_{in})$ is the output voltage of the thermoelectric generator, so the state space expression of the single Buck circuit can be established

$$\mathbf{x} = \mathbf{A}\mathbf{x} + \mathbf{B}\mathbf{u} \quad (7)$$

$$\mathbf{y} = \mathbf{C}\mathbf{x} + \mathbf{D}\mathbf{u} \quad (8)$$

In the formula, the state and input matrix are $\mathbf{A} = (\mathbf{NPQ})^T$, $\mathbf{B} = \left(\frac{1}{C_1 00}\right)^T$, $\mathbf{N} = (0d/L0)^T$, $\mathbf{P} = \left(-\frac{d}{C_1}R(1-2d)/L1/C_2\right)$, $\mathbf{Q} = (0(1-2d)/L - 1/(C_2 R_o))$. In Eq. (8), the output and feedforward matrices are $\mathbf{C} = (100)$, $\mathbf{D} = (0)$ in sequence. According to the single-phase Buck model, the state, input, output and feedforward matrix of the two-phase interleaved Buck circuit are $(2\mathbf{N}2\mathbf{P}2\mathbf{Q})^T$, $(1/C_1 00)^T$, (100) , (0) respectively. A disturbance is added at the steady state point, and the nonlinear AC small-signal state equation of the two-phase interleaved Buck circuit is:

$$\begin{pmatrix} \frac{d\hat{U}_{in}}{dt} \\ \frac{d\hat{i}_L}{dt} \\ \frac{d\hat{U}_o}{dt} \end{pmatrix} = \begin{bmatrix} 000 \\ 000 \\ 000 \end{bmatrix} \begin{bmatrix} \hat{U}_{in} \\ \hat{i}_L \\ \hat{U}_o \end{bmatrix} + \begin{bmatrix} \frac{1}{C_1} \\ 0 \\ 0 \end{bmatrix} I_{in} + \begin{bmatrix} \frac{-\hat{U}_{in}}{C_1} \\ \frac{2(\hat{U}_{in} - 2R\hat{i}_L - 2\hat{U}_o)}{L} \\ 0 \end{bmatrix} \hat{d} \quad (9)$$

Since the equivalent resistance R of the filter inductor is very small, its influence can be ignored, so the transfer function of the DC/DC input voltage to the duty cycle d is:

$$\frac{\hat{U}_{in}(s)}{\hat{d}(s)} = \frac{a_3 s^2 + a_2 s + a_1}{b_3 s^2 + b_2 s + b_1} \quad (10)$$

where $a_3 = I_{in} C_2 R_o L$; $a_2 = I_{in} L$; $a_1 = 2R_o I_{in} (2d - 1)$; $b_3 = d^2 C_1 C_2 R_o$; $b_2 = d^2 (C_1 + 2d C_2 R_o)$; $b_1 = 2d^3$.

A PI controller is designed using the converter element parameters shown in Tab. 1 and the circuit parameters of the thermoelectric generator at rated power to improve the dynamic stability performance of the feedback MPPT control loop.

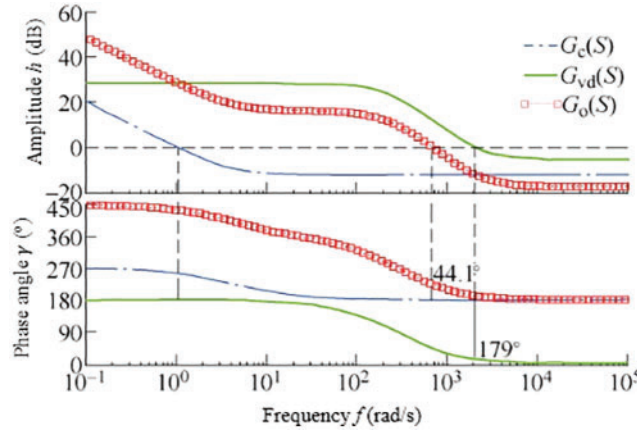
Table 1: Corresponding component parameters of two-phase interleaved parallel Buck DC/DC converters

Parameter	Numerical value
Rated power P	1 kW
Input voltage U_{in}	50~350
Output voltage U_{out}	45~55
Input side capacitance C_1	4700 μF
Output side capacitor C_2	80 μF
Output side inductance L	400 μH

Transfer function of DC/DC input voltage to duty cycle d

$$G_{vd}(s) = \frac{1.344 \times 10^{-6} \times s^2 + 5.6 \times 10^{-4} \times s - 5.04}{2.49 \times 10^{-6} \times s^2 + 1.54 \times 10^{-3} \times s + 0.2} \quad (11)$$

The transfer function of DC/DC input voltage to duty cycle before and after correction is shown in Fig. 6, the cut-off frequency of $G_{vd}(s)$ before correction is 2.05×10^3 rad/s, the phase angle margin $\gamma = -179^\circ$, amplitude margin $h = -28$ dB, the system is unstable. Design a series lag correction link $G_c(s) = (-0.25s+1)/s$ in MATLAB's sisotool, where $K_p = -0.25$, $T_i = -0.25$, the corrected open-loop transfer function $G_o(s) = G_c(s) \times G_{vd}(s)$, $h = 17.4$ dB, $\gamma = 44.1^\circ$, cutoff frequency 681 rad/s, the steady-state performance of the system is greatly improved. The root locus diagram of $G_o(s)$ is shown in Fig. 7, and the adjustment time is $t_s = 4.4/\sigma = 0.76$ s, indicating that the dynamic performance has been improved.

**Figure 6:** Bode plot of $G_{vd}(s)$ before correction and $G_o(s)$ after correction

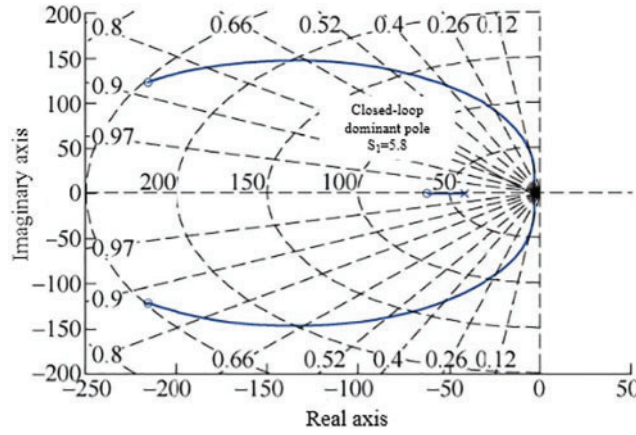


Figure 7: Corrected $G_o(s)$ root locus

3 Proposed Algorithm

3.1 Modified Conductance Incremental Method

Usually, the incremental conductance method adopts a fixed-step strategy, and the selection of the step change ΔD is blind. As shown in Fig. 8, Reference [21] proposed that $D(k+1) = D(k) \pm N \cdot |\Delta P / \Delta V|$, and the scale factors N_1 and N_2 are determined according to curves 1 and 2 in turn. When N_1 is used, curve 1 runs with a fixed step size ΔD_{\max} most of the time, if the temperature of the thermoelectric generator changes, the system will oscillate violently, affecting the tracking efficiency. When N_2 is used, most of the curve 1 runs with variable step size $N \cdot |\Delta P / \Delta V|$, and the response speed is slow, so there is a “dead zone” space for this method.

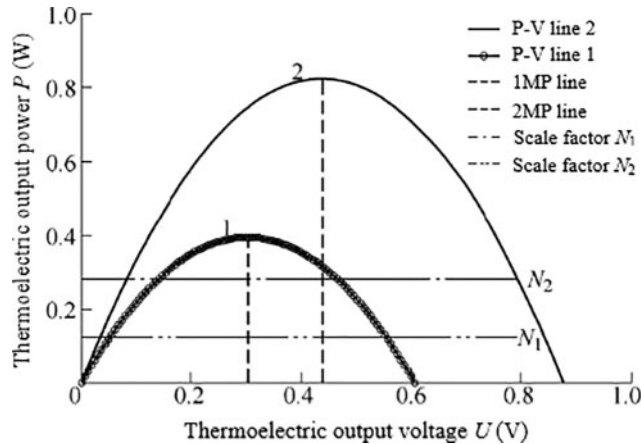


Figure 8: Schematic diagram of variable step size algorithm

In order to solve the problem of the proportional coefficient N of the traditional variable-step conductance increment algorithm, this paper proposes a new improved conductance increment method in the first stage of MPPT. It can be seen from Fig. 9, the curve $C_n = P_n / |\Delta P / \Delta V|$ ($n = 1, 2, 3, \dots$) is symmetrical about the maximum power point of PV curve 1, and the change trend on MPP is to increase first and then decrease. At the same time, with the increase of n , the extreme

point of C_n is closer to the maximum power point of curve 1, but the amount of calculation increases exponentially. When $n = 3$, the algorithm tracks the maximum power better, and requires the DSP chip TMS320F28335 to calculate moderately. The specific process is as follows

$$\left\{ \begin{array}{ll} \frac{dC_3}{dV} > 0 \cap \frac{dP}{dV} > 0 & D(k+1) = D(k) - |\Delta D_{\max}| \\ \frac{dC_3}{dV} \leq 0 \cap \frac{dP}{dV} > 0 & D(k+1) = D(k) - |\Delta D_{\text{ANN}}| \\ \frac{dC_3}{dV} > 0 \cap \frac{dP}{dV} < 0 & D(k+1) = D(k) + |\Delta D_{\text{ANN}}| \\ \frac{dC_3}{dV} \leq 0 \cap \frac{dP}{dV} < 0 & D(k+1) = D(k) + |\Delta D_{\max}| \end{array} \right. \quad (12)$$

In the formula, ΔD_{\max} is the maximum step size change in the MPPT process, and ΔD_{ANN} is the output value of the second-stage adaptive variable step size BP neural network method.

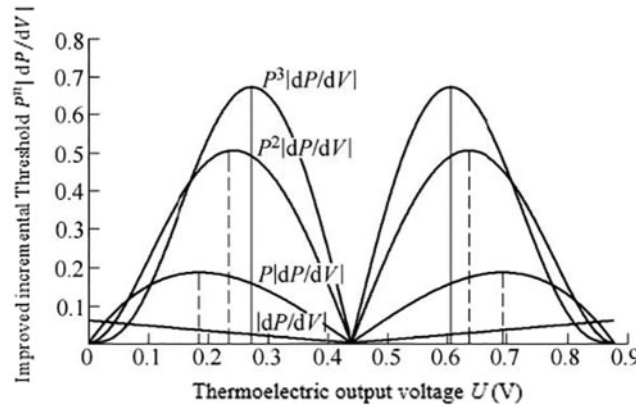


Figure 9: Schematic diagram of the improved variable-step conductance increment method

3.2 Adaptive Variable Step Size BP Neural Network Method

The advantage of a neural network is that it does not require an accurate mathematical model, but it can establish complex nonlinear relationships between input and output. In this paper, the feedforward BP-ANN method is adopted. There are three-layer networks. The transfer functions of the hidden layer and the output layer are tansig and purelin. The neural structure is trained by the gradient descent method. The input layer has two neurons, the hidden layer has 5 neurons, and the output layer consists of only one neuron. As shown in Fig. 10, the two input quantities are the change dV of the output voltage of the thermoelectric generator and the change dP of the output power, and the output quantity is the increase or decrease of the normalized duty cycle (± 1).

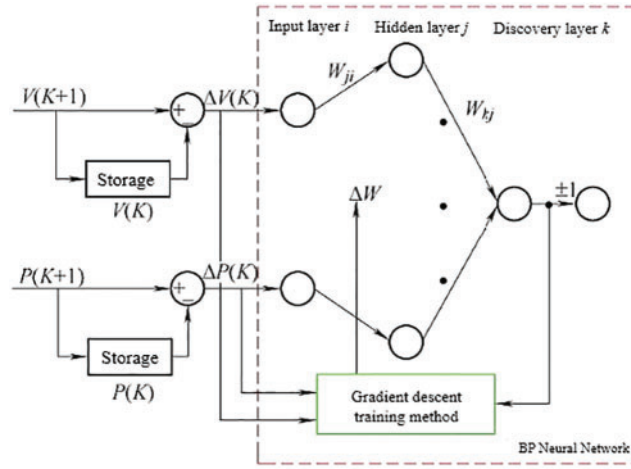


Figure 10: Proposed BP neural network configuration

In order to adjust the weights, according to the gradient descent method, the formula is as follows

$$\begin{cases} \Delta W_{ji} = \eta \cdot \frac{\partial E}{\partial net_j} \cdot o_i \\ \Delta W_{kj} = \eta \cdot \frac{\partial E}{\partial net_k} \cdot o_k \end{cases} \quad (13)$$

where η is the learning rate; E is the error between the actual output and the expected output; net_j , net_k are the input of neurons in the hidden layer and output layer respectively; o_i and o_k are the outputs of neurons in the input layer and hidden layer, respectively.

The neural network established in MATLAB is shown in Fig. 11. After 444 training iterations, the root mean square error (RMSE) can reach 6.86×10^{-3} .

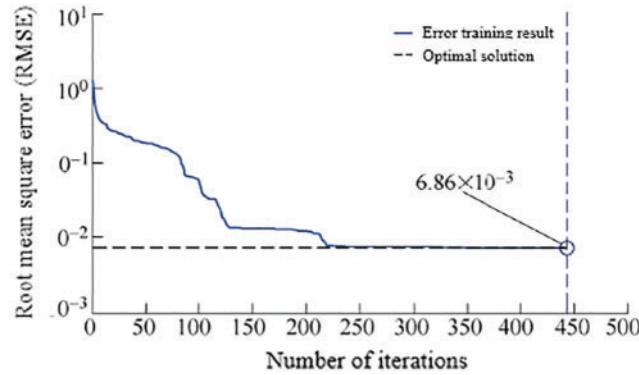


Figure 11: Error training result

The adopted BP neural network method operates in two modes: Offline and online. Firstly, in offline mode, collect 200 sets of experimental data of the conductance incremental method with a fixed step size $\Delta D = 0.001$ under a fixed external condition, use the back-propagation algorithm to train the data, and find a suitable neural network structure. Then, the online mode uses the offline BP

neural network for MPPT. The basic principle of MPPT of BP neural network method is shown in the following formula

$$\begin{cases} dP > 0 \cap dV > 0 & Out_{ANN} = -1 \\ dP > 0 \cap dV < 0 & Out_{ANN} = +1 \\ dP < 0 \cap dV > 0 & Out_{ANN} = +1 \\ dP < 0 \cap dV < 0 & Out_{ANN} = -1 \end{cases} \quad (14)$$

When the on-board thermoelectric generator is running in a steady state, the temperature of the exhaust pipe and the output power of the thermoelectric generator do not change or change slowly. When the operating conditions of the engine suddenly change, the temperature and flow rate of the exhaust gas will change drastically, resulting in a sudden change in the output power of the thermoelectric generator. If the traditional fixed-step BP neural network method is used to find the new maximum power point, the dilemma of slow convergence speed and steady-state oscillation will occur. Because choosing a larger step size can ensure that the dynamic time is shortened, but steady-state oscillation is inevitable. Choosing a smaller step size can reduce steady-state oscillation, but it will be accompanied by the problem of poor dynamic performance. In order to account for the on-board thermoelectric generator's tracking speed and steady-state accuracy, this paper proposes an adaptive variable step size adjustment strategy according to the power variation characteristics of the on-board thermoelectric generator, as shown below.

$$D(K) = D(K-1) \pm (C + e^{-|dP|^2}) \quad (15)$$

$$\begin{cases} C = C_{\max} e^{-|dP|^2} \leq \alpha_{\min} \\ C = \frac{(e^{-|dP|^2} - \alpha_{\min}) \cdot (C_{\max} - C_{\min})}{\alpha_{\max} - \alpha_{\min}} + C_{\min} \alpha_{\min} < e^{-|dP|^2} < \alpha_{\max} \\ C = C_{\min} e^{-|dP|^2} \geq \alpha_{\max} \end{cases} \quad (16)$$

In the formula, $D(K)$ and $D(K-1)$ are the duty ratios of the switches at time K and $K-1$, respectively. $e^{-|dP|^2}$ is the step size change dimensioning factor; α_{\max} and α_{\min} are the upper and lower thresholds of the set dimensioning factor, respectively; C is the step change adjustment factor; C_{\max} and C_{\min} are the maximum and minimum adjustment factors, respectively. The adaptive variable step size adjustment strategy proposed in this paper is more reliable than the online mode variable step size method proposed by [22]. If the second stage of the maximum power tracking of the on-board thermoelectric power generation adopts the online mode variable step method [22], that is, $\Delta D = E + M \cdot dP$, where E is the fixed step value, and M is the proportional coefficient. With the change of engine operating conditions, the output power of the thermoelectric generator also changes, which leads to blindness in the selection of M . In addition, the step size change dimensionalization factor $e^{-|dP|^2}$ used in this paper replaces the power change dP of [22], and the value range of the adjustment factor C is narrowed, which can avoid the divergence of the MPPT controller.

In the adaptive variable step size adjustment strategy, the dimensioning factor $e^{-|dP|^2}$ can reflect the change speed of the output power of the on-board thermoelectric power generation in real time. When the dimensioning factor $e^{-|dP|^2}$ is between the upper threshold α_{\max} and the lower threshold α_{\min} , it is considered that the state of the thermoelectric generator has undergone a moderate change, and the adjustment factor C can be adaptively changed according to the speed of the output power change.

To sum up, a new hybrid MPPT algorithm is proposed as shown in Fig. 12.

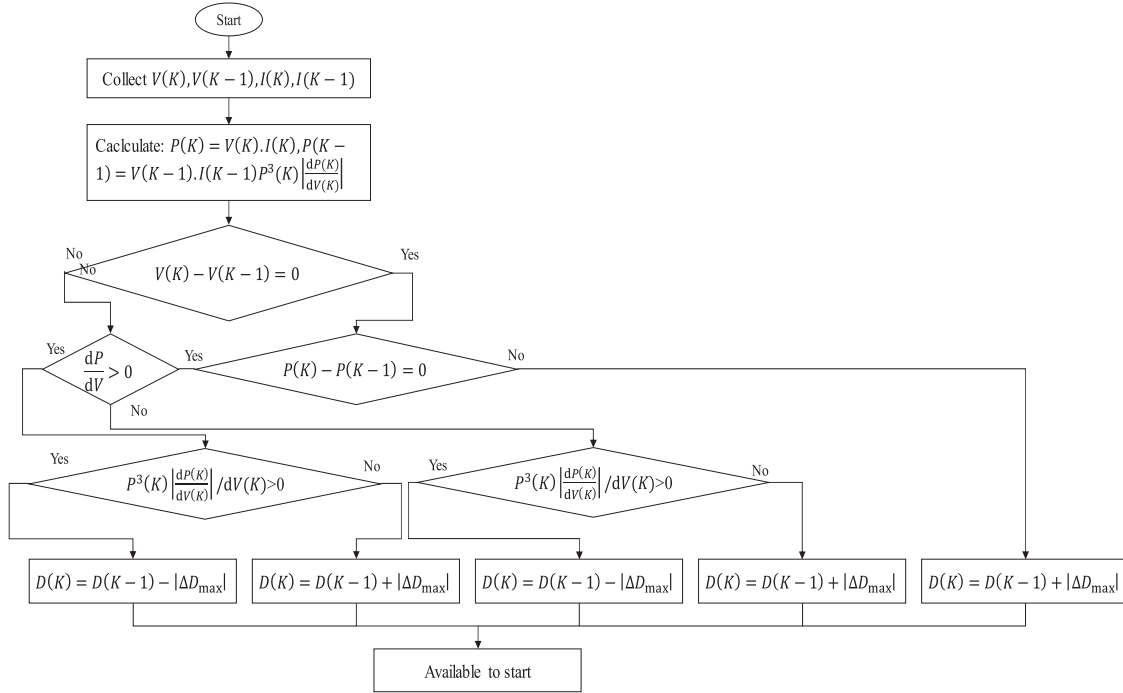


Figure 12: Proposed control algorithm flowchart

4 Simulation and Experimental Analysis

4.1 MATLAB/Simulink Modeling

The equivalent circuit model of a single thermoelectric module is a voltage source connected in series with a resistor, and its output is related to the temperature difference between the hot and cold ends. As shown in Fig. 13, the Simulink model of the thermoelectric generator consists of 60 thermoelectric modules (Bi2Te3) connected in series.

Set the initial temperature difference of the thermoelectric generator $\Delta T_1 = 198.7^\circ\text{C}$, change to $\Delta T_2 = 94.7^\circ\text{C}$ at 3 s, then jump to $\Delta T_3 = 198.7^\circ\text{C}$ at 6 s, and finally change to $\Delta T_1 = 57.9^\circ\text{C}$ at $t = 10$ s. In order to compare the performance of each method more precisely, this paper uses three criteria that is, MPPT tracking accuracy, response time, and overshoot.

4.2 Simulation Results

The simulation results of the proposed algorithm, the separate improved conductance incremental method (SIINC) and the separate BP artificial neural network method (SBP-ANN) are shown in Figs. 14–16. Fig. 14 shows the simulation waveforms of the tracking accuracy of the three MPPT algorithms. It can be seen that when the temperature difference of the thermoelectric generator is $\Delta T = 198.7^\circ\text{C}$, the average tracking powers of HM, SBP-ANN and SIINC are 205.3, 205.2, and 203.6 W in turn. At the same time, when the thermoelectric generator temperature difference $\Delta T = 94.7^\circ\text{C}$, the average power values of HM, SBP-ANN and SIINC tracking are 97.9, 97.7, 95.3 W in turn.

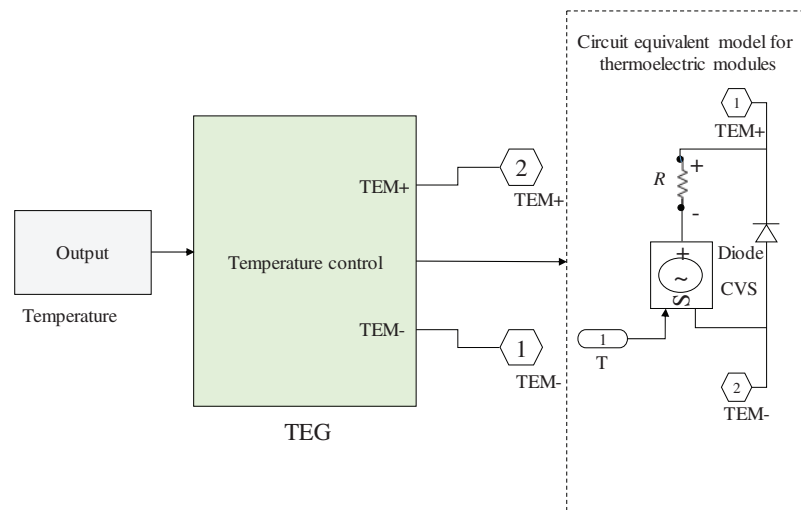


Figure 13: Simulink model of thermoelectric generator

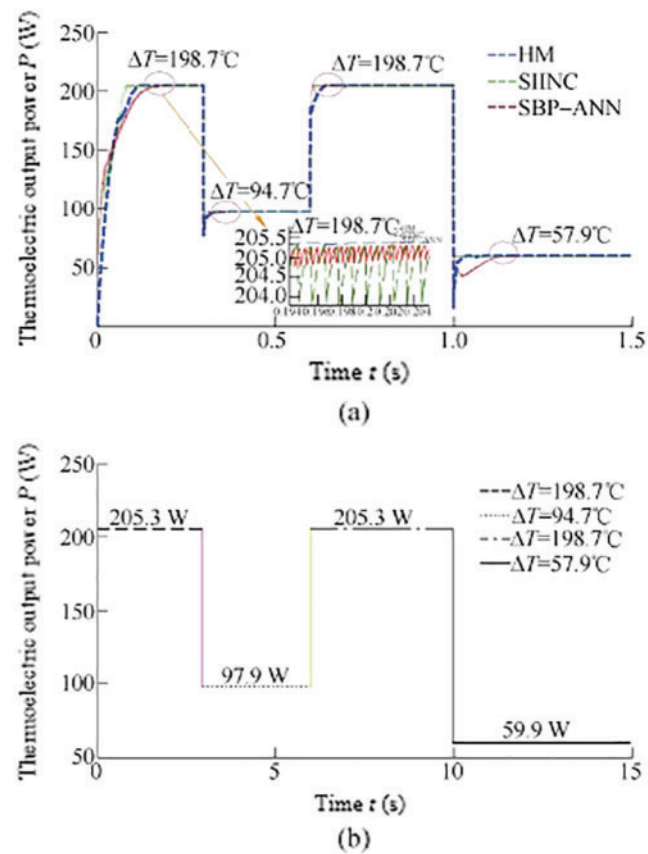


Figure 14: Comparison of the MPPT tracking accuracy for the algorithms

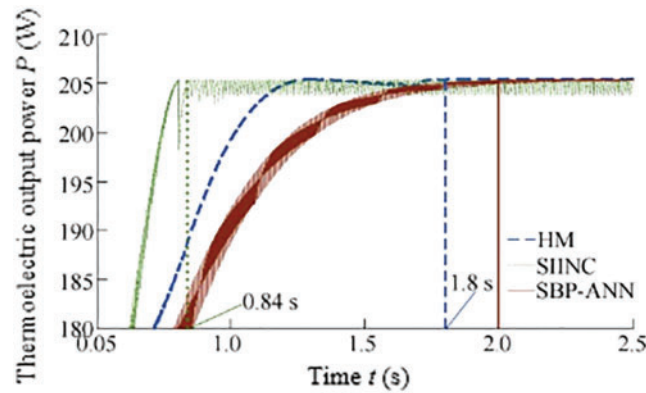


Figure 15: Comparison of the MPPT response time of the algorithms

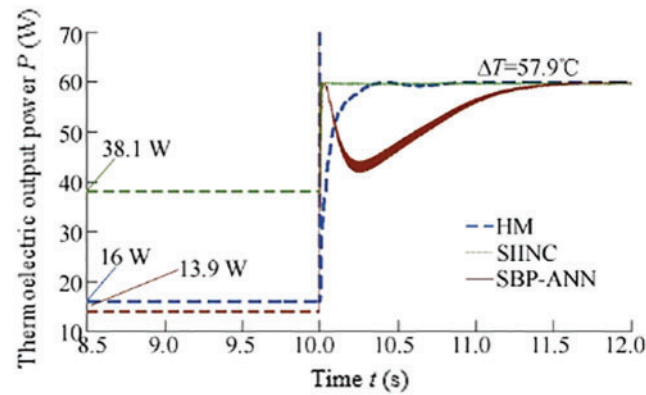


Figure 16: Comparison of the MPPT overshoot for the algorithms

It shows that the HM and SBP-ANN search for the maximum power is very close to the theoretical value, and the steady-state accuracy is very high. However, when SIINC tracks the maximum power, the duty cycle of the DC/DC converter changes drastically, resulting in a lot of power loss, so its steady-state accuracy is not high.

As shown in Fig. 15, when ΔT is from 0°C to 198.7°C , the response times of HM, SIINC and SBP-ANN for tracking the maximum power are 1.8 s, 0.84 s and 2 s respectively. It shows that in each switching cycle, the SIINC adopts the largest step size change, so the startup time and response time are the shortest, and the HM proposed in this paper combines the advantages of SBP-ANN and SIINC, and has good startup speed and response speed. However, the SBP-ANN collects the experimental data of the conductance increment method with a fixed step size $\Delta D = 0.001$, and the duty cycle of the DC/DC converter changes the slowest, so its response time is the longest.

As shown in Fig. 16, when ΔT is from 198.7°C to 57.9°C , the overshoot of HM tracking the maximum power (43.9 W) is 2.01 times that of SIINC (21.8 W) and 0.95 times that of SBP-ANN (46 W). It shows that the dynamic performance of the proposed HM algorithm is worse than that of SBP-ANN, but not as good as SIINC. For SIINC, when the temperature is abruptly changed, its step size change ΔD is the smallest, so its overshoot is the smallest and the dynamic performance is the best.

4.3 Test Results Evaluation

In order to verify the effectiveness of the proposed HM algorithm, a test bench was created for AETEG which is depicted in Fig. 17, the car engine model is Citroen Seg a 2.0 PSA RFN 10LH3X, the capacity is 1997 mL, the maximum power is 108 kW (6000 r/min), the maximum Torque 200 NM (4000 r/min). The heat conduction area of the heat energy air box is 542 mm \times 280 mm, and the cooling area of the cold source water tank is also 542 mm \times 280 mm. The material of the thermoelectric module is Bi₂Te₃, and the number is 60. The rated power of the DC/DC converter is 1 kW, and the specific parameters are shown in Tab. 1. Following the steady-state tracking test, the thermoelectric generator is directly connected to the electronic load, and the true maximum power of the thermoelectric generator is determined using the current sweep method. The thermoelectric generator is then linked to the 48 V battery through the DC/DC converter included into the MPPT algorithm. Secondly, we performed dynamic tracking experiment. At 1.6 s, the speed and torque of the car engine jump from 3000 r/min@65NM to 2600 r/min@58NM. The proposed HM algorithm and the traditional SIINC, SBP-ANN algorithms are embedded into the digital controller TMS320F28335, its PWM module outputs the drive signal to the IGBT device to realize the MPPT algorithm.

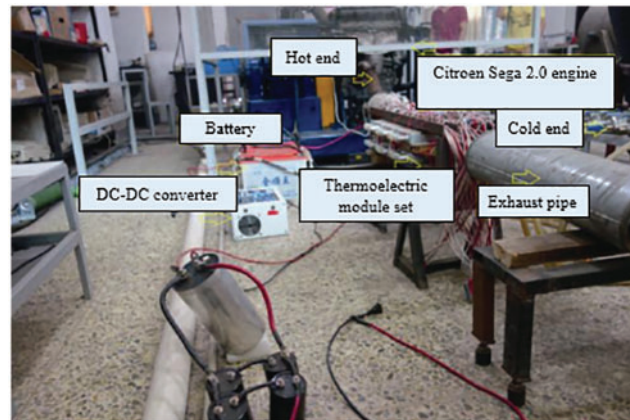


Figure 17: AETEG test bench with embedded MPPT algorithm

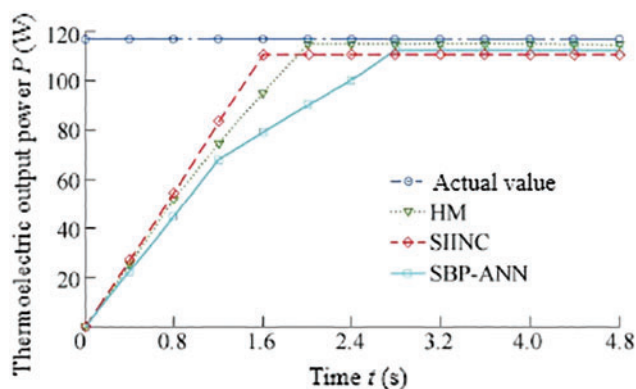
When the automobile engine runs in two stable conditions (3000 r/min@65NM, 2600 r/min@58NM), the results are shown in Tabs. 2 and 3 and Figs. 18 and 19. As shown in Fig. 18, the maximum tracking powers of HM, SIINC and SBP-ANN are 114.87 W, 110.49 W and 112.45 W in turn, and the deviation rate of the proposed algorithm is the smallest (1.53%), indicating that it's steady-state accuracy is the highest and consistent with the simulation results. Due to the existence of actual circuit losses (switching losses of switching tubes, impedance losses of wires), the MPPT result has a certain error with the actual value.

Table 2: Comparison of algorithms results under 3000 r/min@65NM conditions

Factor	Actual value	SIINC algorithm	SBP-ANN algorithm	Proposed
Hot end temperature T_H (°C)	226.9	226.9	226.9	226.9
Cold end temperature T_c (°C)	62.4	62.4	62.9	62.4
Voltage U (V)	100.4	100.4	100.4	100.4
Current I (A)	1.16	1.08	1.07	0.94
Power P (W)	116.66	110.49	112.45	114.87
Deviation rate e (%)	0	5.28	3.61	1.53

Table 3: Comparison of algorithms results at 2600 r/min@58NM

Factor	Actual value	SIINC algorithm	SBP-ANN algorithm	Proposed
Hot end temperature T_H (°C)	105.1	105.1	105.1	105.1
Cold end temperature T_c (°C)	59.5	59.5	59.5	59.5
Voltage U (V)	50.7	63.8	82.5	57.2
Current I (A)	0.79	0.56	0.46	0.68
Power P (W)	40.1	35.9	37.9	39.2
Deviation rate e (%)	0	10.4	5.50	2.24

**Figure 18:** The actual output of AETEG and the results of different MPPT algorithms at 3000 r/min@65 NM

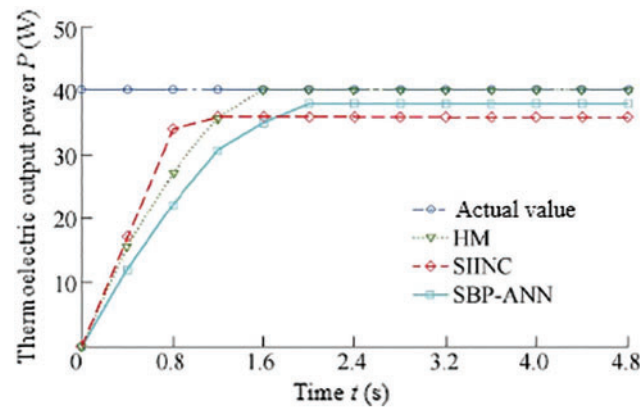


Figure 19: The actual output of AETEG and the results of different MPPT algorithms at 2600 r/min@58 NM

As shown in Fig. 19, the HM, SIINC and SBP-ANN algorithms find the maximum powers to be 39.2, 35.9 and 37.9 W respectively. In addition, when the engine speed and torque suddenly change from 0 to 3000r/min@65NM, the maximum power tracking start time of the proposed algorithm is 2 s, which is 0.4 s more than SIINC but 0.8 s less than the SBP-ANN algorithm, indicating that the starting speed and response speed of the suggested approach is a hybrid of SIINC and SBP-ANN, which matches the simulation findings. Since BP-ANN is used in the second stage of the proposed algorithm, its step size change is smaller than the ΔD of SIINC method, so the startup time is not as good as SIINC (See Fig. 20).

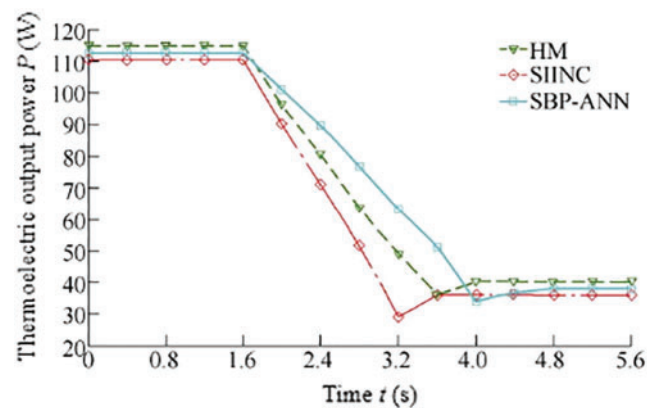


Figure 20: The results of different MPPT algorithms when the speed and torque of the car engine jumped from 3000 r/min@65 NM to 2600 r/min@58 NM

Among them, the response times of proposed, SIINC and SBP-ANN algorithms are 2.4, 2 and 3.2 s, indicating that SIINC has the shortest dynamic response time, but its overshoot of 5.9 W is greater than 2.1 W of proposed algorithm and 3.8 W of SBP-ANN algorithm, causing great damage to the circuit components of the DC/DC converter. The experimental results show that the proposed algorithm outperforms the traditional SIINC and SBP-ANN algorithms in terms of stability and dynamic performance.

5 Conclusion

This paper proposed a novel algorithm for thermoelectric generator based on neural networks.

(1) The AETEG system based on the 48 V electrical architecture is proposed, which can improve the fuel economy of the vehicle and achieve the effect of energy saving and emission reduction.

(2) The design and implementation of the double closed-loop interleaved Buck converter ensures the high efficiency and stability of the AETEG system.

(3) Based on the maximum power tracking strategy, the improved conductance increment method can be used when far from the maximum power point, which can improve the dynamic performance of the system. When approaching the maximum power point, the adaptive variable step size BP neural network method can reduce the steady-state oscillation.

(4) Simulation and experimental results show that the hybrid method proposed in this paper can not only improve the output power of the on-board thermoelectric generator, but also reduce the response time of the system.

Acknowledgement: The authors would like to thanks the editors and reviewers for their review and recommendations.

Funding Statement: The authors received no specific funding for this study.

Conflicts of Interest: The authors declare that they have no conflicts of interest to report regarding the present study.

References

- [1] S. Twaha, J. Zhu, L. Maraaba, K. Huang, B. Li *et al.*, "Maximum power point tracking control of a thermoelectric system using the extremum seeking control method," *Energies Journal*, vol. 10, no. 12, pp. 1–18, 2017.
- [2] S. Kim, S. Park and K. Kim, "A thermoelectric generator using engine coolant for light-duty internal combustion engine-powered vehicles," *Journal of Electronic Materials*, vol. 24, no. 5, pp. 812–816, 2011.
- [3] H. Mamur, M. Ustuner and M. Bhuiyan, "Future perspective and current situation of maximum power point tracking methods in thermoelectric generators," *Sustainable Energy Technologies and Assessment Journal*, vol. 50, no. 3, pp. 742–763, 2022.
- [4] T. Zhang, "New thinking on modeling of thermoelectric devices," *Applied Energy*, vol. 168, no. 7, pp. 65–74, 2016.
- [5] W. He, W. Wang and Y. Yang, "Peak power evaluation and optimal dimension design of exhaust heat exchanger for different gas parameters in automobile thermoelectric generator," *Energy Conversion and Management*, vol. 151, no. 3, pp. 661–669, 2017.
- [6] M. Comamala, I. Cozar, A. Massaguer, E. Massaguer and T. Puiol, "Effects of design parameters on fuel economy and output power in an automotive thermoelectric generator," *Energies Journal*, vol. 11, no. 12, pp. 1–18, 2018.
- [7] I. Cozar, T. Puiol and M. Lehocky, "Numerical analysis of the effects of electrical and thermal configurations of thermoelectric modules in large-scale thermoelectric generators," *Applied Energy Journal*, vol. 299, no. 6, pp. 264–280, 2018.
- [8] A. Abdullah, H. Rezk, A. Alboye, M. Hassan and A. Mohamed, "Grey wolf optimizer-based fractional MPPT for thermoelectric generator," *Intelligent Automation & Soft Computing*, vol. 29, no. 3, pp. 729–740, 2021.
- [9] A. Jordehi, "Maximum power point tracking in photovoltaic (PV) systems: A review of different approaches," *Renewable and Sustainable Energy Reviews*, vol. 65, no. 1, pp. 1127–1138, 2016.

- [10] C. Li, Y. Chen, D. Zhou, J. Liu and J. Zeng, "A high-performance adaptive incremental conductance MPPT algorithm for photovoltaic systems," *Energies Journal*, vol. 9, no. 4, pp. 1–16, 2016.
- [11] H. Islam, S. Mekhilef, N. Shah, T. Soon and M. Seyed, "Performance evaluation of maximum power point tracking approaches and photovoltaic systems," *Energies Journal*, vol. 9, no. 8, pp. 1043–1063, 2015.
- [12] L. Elobaid, A. Abdelsalam and E. Zakzouk, "Artificial neural network-based photovoltaic maximum power point tracking techniques: A survey," *IET Renewable Power Generation*, vol. 9, no. 8, pp. 1043–1063, 2015.
- [13] A. Dounis, P. Kofinas and G. Papadakis, "A direct adaptive neural control for maximum power point tracking of photovoltaic system," *Solar Energy*, vol. 115, no. 5, pp. 145–165, 2015.
- [14] H. Yamada, K. Kimura and T. Hanamoto, "A novel MPPT control method of thermoelectric power generation with single sensor," *Applied Sciences*, vol. 3, no. 2, pp. 545–558, 2013.
- [15] Z. Dalala and M. Saadeh, "A new maximum power point tracking (MPPT) algorithm for thermoelectric generators with reduced voltage sensors count control," *Energies Journal*, vol. 11, no. 7, pp. 1826–1841, 2018.
- [16] D. Tatarinov, M. Koppers and G. Bastian, "Modeling of a thermoelectric generator for thermal energy regeneration in automobiles," *Journal of Electronic Materials*, vol. 42, no. 7, pp. 2274–2281, 2013.
- [17] Y. Deng, S. Zheng and C. Su, "Effect of thermoelectric modules topological connection on automotive exhaust heat recovery system," *Journal of Electronic Materials*, vol. 45, no. 3, pp. 1740–1750, 2016.
- [18] J. Gao, K. Sun and L. Ni, "A thermoelectric generation systems and its power electronics stage," *Journal of Electronic Materials*, vol. 41, no. 6, pp. 1043–1050, 2012.
- [19] R. Tan, "Design of boost converter based on maximum power point resistance for photovoltaic applications," *Solar Energy*, vol. 160, no. 7, pp. 322–335, 2018.
- [20] C. Jiang and H. Liu, "A novel interleaved parallel bidirectional dual-active-bridge dc-dc converter with coupled inductor for more-electric aircraft," *IEEE Transactions on Industrial Electronics*, vol. 68, no. 2, pp. 1759–1768, 2021.
- [21] A. Osadrahimi and Y. Mahmoud, "Novel spline-MPPT technique for photovoltaic systems under uniform irradiance and partial shading conditions," *IEEE Transactions on Sustainable Energy*, vol. 12, no. 1, pp. 524–532, 2020.
- [22] S. Messalti, A. Harrag and A. Loukriz, "A new variable step size neural networks MPPT controller: Review, simulation and hardware implementation," *Renewable and Sustainable Energy Reviews*, vol. 68, no. 2, pp. 221–233, 2017.